

Spatial Distribution and Kinematics of OB Stars

G. A. Gontcharov*

June 30, 2016

Pulkovo Astronomical Observatory, Russian Academy of Sciences, Pulkovskoe sh. 65, St. Petersburg, 196140 Russia

Key words: star counts; distribution of stars; Hertzsprung–Russell diagram; main sequence; early types (O and B); stellar kinematics; Galactic solar neighborhood.

The sample of 37 485 suspected OB stars selected by Gontcharov (2008) from the Tycho-2 catalogue has been cleaned of the stars that are not of spectral types OV–A0V. For this purpose, the apparent magnitude V_T from Tycho-2, the absolute magnitude M_{V_T} calibrated as a function of the dereddened color index $(B_T - V_T)_0$, the interstellar extinction A_{V_T} calculated from the 3D analytical model by Gontcharov (2009) as a function of the Galactic coordinates, and the photometric distance r_{ph} calculated as a function of V_T , M_{V_T} , and A_{V_T} have been reconciled in an iterative process. The 20 514 stars that passed the iterations have $(B_T - V_T)_0 < 0$ and $M_{V_T} > -5$ and are considered as a sample of OV–A0V stars complete within 350 pc of the Sun. Based on the theoretical relation between the dereddened color and age of the stars, the derived sample has been divided into three subsamples: $(B_T - V_T)_0 < -0.2^m$, $-0.2^m < (B_T - V_T)_0 < -0.1^m$, and $-0.1^m < (B_T - V_T)_0 < 0^m$, younger than 100, 100 – 200, and 200 – 400 Myr, respectively. The spatial distribution of all 20 514 stars and the kinematics analyzed for more than 1500 stars with radial velocities from the PCRV and RAVE catalogues are different for the subsamples, showing smooth rotations, shears, and deformations of the layer of gas producing stars with the formation of the Gould Belt, the Great Tunnel, the Local Bubble, and

*E-mail: georgegontcharov@yahoo.com

other structures within the last 200 Myr. The detected temporal variations of the velocity dispersions, solar motion components, Ogorodnikov–Milne model parameters, and Oort constants are significant, agree with the results of other authors, and show that it is meaningless to calculate the kinematic parameters for samples of stars with uncertain ages or with a wide range of ages.

INTRODUCTION

Stars of spectral types O and B are interesting primarily as young high-luminosity stars. The youth, i.e., the short lifetime near the main sequence (MS), is explained by the large mass of OB stars. They exist only in regions of current or recent star formation, for example, in Galactic spiral arms, and, therefore, are good tracers of young and short-lived structures as well as the spatial distribution of the gas from which they have recently been formed. The kinematics retained during their short lifetime is important for understanding the evolution of the Galaxy.

OB stars are convenient for selection, because they have approximately the same metallicity and, consequently, a unique theoretical relation between their mass, dereddened color, absolute magnitude, and age. To illustrate this relation, Fig. 1 shows some evolutionary tracks and isochrones on a Hertzsprung–Russell (H–R) diagram of the form “color ($B_T - V_T$) – absolute magnitude M_{V_T} ” (here and below, all tracks and isochrones were taken from the database in Padova (<http://stev.oapd.inaf.it/cmd>; Bertelli et al. 2008; Marigo et al. 2008); B_T and V_T are the magnitudes from the Tycho-2 catalogue (Høg et al. 2000).

In the figure, the theoretical isochrones for solar metallicity stars with ages of 1, 100, 200, 300, and 400 Myr are indicated by five solid black lines from left to right, respectively. The diamonds with the gray curve passing through them and the squares indicate the evolutionary tracks for a solar-metallicity star with a mass of $2.9 M_\odot$ (on the zero-age main sequence (ZAMS), this is a B7V star) and a star with a mass of $2 M_\odot$ (A0V on the ZAMS), respectively. We see that in this part of the diagram the tracks and isochrones are far from coincidence and the selection of stars larger than some mass is not the same as the selection of stars younger than some age. On the other hand, we see that the B and A stars separate rather clearly near $(B_T - V_T)_0 = 0$. This means that, without oversimplifying, stars with a mass on the MS greater than $2.5 M_\odot$ can be said to be high-luminosity stars younger than 400 Myr; they are also OB stars (including a small fraction of subgiants, giants, and supergiants) and, in the absence of extinction, have $(B_T - V_T)_0 < -0.05$ near the MS. Given the accuracy of the photometry, $\sigma((B_T - V_T)_0) \approx 0.05$, below we select stars with $(B_T - V_T)_0 < 0$ for the sample to be complete.

It can also be seen from the figure that, in contrast to the A stars, the OB stars rapidly change their color to red after core hydrogen exhaustion, i.e., at the subgiant stage. Therefore, theoretically, the upper right quarter

of the shown diagram must be devoid of stars.

Thus, the task is seemingly simple – the selection of OB stars as the bluest stars. However, some of the low-mass stars at the core helium burning stage (hot subdwarfs, blue horizontal-branch halo and thickdisk stars) (Gontcharov et al. 2011) and extremely fast OB stars (Tetzlaff et al. 2011) have the same color and absolute magnitude. They can be revealed only by their spectroscopy and kinematics. In addition, even a slight extinction leads to such a reddening of an OB star that it has color indices approximately as those for stars of type A or even later.

Gontcharov (2008a) showed that the set of five photometric bands, B_T and V_T from Tycho-2 and J , H , and K_s from the 2MASS catalogue (Skrutskie et al. 2006), is sufficient for the separation of OB and later-type stars on colorcolor ($V_T - H$) - ($J - K_s$) diagrams, although some admixture of extraneous stars remains. In this case, the spectral classification of stars is not used at all. All stars in the region of the color-color diagram determined relative to the ZAMS and the theoretical reddening line for B5 stars are deemed OB stars. As a result, a sample of 37 485 suspected OB stars from the Tycho-2 catalogue was produced. Comparison with the well-known spectral classification from the Hipparcos Input Catalogue (HIC, Turon et al. 1993) and Tycho-2 Spectral Types (TST) catalog (Wright et al. 2003) confirms that the selected stars are of types OB with an admixture of later types. This admixture forces the sample by Gontcharov (2008a) to be considered as a preliminary one.

Smaller but cleaner samples of OB stars were produced on its basis *by invoking the well-known spectral classification*: a sample of 15 670 stars to construct the 3D analytical extinction model (Gontcharov 2009) and a sample of 11 990 stars to investigate the spatial variations of the extinction coefficient R_V (Gontcharov 2012a). However, as was shown by Gontcharov (2008a), using the well-known spectral classification causes strong observational selection and does not allow the spatial distribution of OB stars to be investigated. In addition, it can be seen from our comparison of the sample sizes (37 485 stars against 15 670 and 11 990) that doubts about whether the stars belong to OB ones arise for most stars of the preliminary sample.

For the stars of the preliminary sample with accurate parallaxes π and proper motions μ from the Hipparcos catalogue (ESA 1997), Gontcharov (2008a) found the correlation $M_{V_T} = 0.45M'_{V_T} - 1$ between the absolute magnitude M_{V_T} and the reduced proper motion $M'_{V_T} = V_T - A_{V_T} + 5 + 5 \cdot \lg(\mu)$, where A_{V_T} is the extinction in the V_T band estimated by Gontcharov

(2008a) for each star from its color index, $\mu = (\mu_\alpha \cos \delta^2 + \mu_\delta^2)^{1/2}$ is the total proper motion in arcseconds. This correlation is explained by the correlation between π and μ in the absence or consideration of systematic motions of the stars relative to the Sun and in the absence of observational selection. For example, Gontcharov (2008a) took into account the Galactic rotation and the solar motion to the apex. As a result, for each star of the sample we can calculate the distance

$$r_{rpm} = 10^{(V_T - A_{V_T} - (0.45M_{V_T}' - 1) + 5)/5}, \quad (1)$$

Gontcharov (2008a) called it the photometric one, although here and below it would be more correct to call it the photoastrometric one, following the authors of the Besancon model of the Galaxy (BMG, Robin et al. 2003), as distinct from the classical definition of the photometric distance via the calibration of M_{V_T} as a function of $((B_T - V_T)_0)$. Such a calibration for the stars of the preliminary sample is performed below. This allowed us to calculate the photometric distances

$$r_{ph} = 10^{(V_T - A_{V_T} - M_{V_T} + 5)/5}, M_{V_T} = f((B_T - V_T)_0) \quad (2)$$

where f is the function found below.

Using r_{rpm} for OB stars is restricted by the fact that because of their youth, the assumption about the absence of systematic motions is invalid and no accurate allowance for these motions is possible. Therefore, Gontcharov (2008a) reached only general conclusions about the spatial distribution and kinematics of OB stars. This paper is devoted to their detailed analysis based on r_{ph} and not on r_{rpm} . We calculate r_{ph} , eliminate the admixtures of extraneous stars, divide the sample into subsamples of stars with different ages, and study in detail their spatial distribution and kinematics.

PHOTOMETRIC DISTANCES

Let us estimate the accuracies of the quantities in Eq. (2). V_T is known from observations with an accuracy that, as a rule, is better than 0.1^m . M_{V_T} depends on $(B_T - V_T)_0$. As Perryman (2009) showed, the scatter of individual values of M_{V_T} around this dependence for stars of the same spectral subtype and luminosity class is usually larger than 0.5^m . In turn, $(B_T - V_T)_0$ depends on B_T , V_T , and A_{V_T} . The extinction A_{V_T} can be determined by various methods, but we imply either a certain spectral energy distribution for a given star

in the absence of extinction or a certain mean extinction in a given region of space. The accuracy of calculating the extinction $\sigma(A_{V_T})$ for a specific star is determined by the scatter of the spectral energy distributions for stars of the same type in the former case and by the scatter of the individual extinctions for neighboring stars in the latter case. As was shown by Gontcharov (2011), $\sigma(A_{V_T}) \approx 0.3^m$ within the nearest kiloparsec in both cases. Consequently, the accuracy of determining r_{ph} from Eq. (2) depends primarily on the accuracy of determining M_{V_T} . Therefore, the method of determining A_{V_T} is not so important and we can relate all quantities in Eq. (2) cyclically by admitting the dependence of A_{V_T} on r_{ph} (as well as on l and b) according to the 3D analytical extinction model (Gontcharov 2009) by taking into account the relation $A_{V_T} = 1.1A_V$ in accordance with the most commonly used extinction laws, for example, from Rieke and Lebofsky (1985). When calculating the parameters of the extinction model, Gontcharov (2009) used both OB stars and stars of other types (Gontcharov 2012b). Therefore, the model is valid for all stars.

Thus, using the 3D model to estimate A_{V_T} allows M_{V_T} , r_{ph} , and A_{V_T} for most stars of the preliminary sample to be reconciled in an iterative process, with the minority of extraneous stars having been thrown away.

$M_{V_T} = f((B_T - V_T)_0)$ Calibration

When calibrating M_{V_T} as a function of $(B_T - V_T)_0$

$$M_{V_T} = V_T + 5 - 5 \lg(r_{HIP}) - A_{V_T}, \quad (3)$$

where $A_{V_T} = 1.1A_V$, and A_V was calculated from the mentioned 3D extinction model

$$(B_T - V_T)_0 = (B_T - V_T) - E_{(B_T - V_T)}, \quad (4)$$

where the reddening $E_{(B_T - V_T)}$ was also calculated from the 3D extinction model and the 3D map of R_V variations (Gontcharov 2012a): $E_{(B_T - V_T)} = 1.1A_V/R_V$. For the calibration, we used all 3237 stars of the preliminary sample with parallaxes $\pi > 5$ mas from the new version of Hipparcos (van Leeuwen 2007), provided that the relative accuracy of the parallax $\sigma(\pi)/\pi < 0.2$. The limitations stem from the fact that the Lutz–Kelker and Malmquist biases (Lutz and Kelker 1973; Perryman 2009, pp. 209–211) did not manifest themselves only for the stars nearer than 200 pc.

Figure 1a shows the positions of 3237 calibration stars on the $(B_T - V_T) - M_{V_T}$ diagram, where the color was not dereddened. Figure 1b shows the positions of the same stars on the $(B_T - V_T)_0 - M_{V_T}$ diagram, i.e., after dereddening. We see that the overwhelming majority of stars are placed by the applied extinction model in the expected region between the 1-Myr isochrone and the “loops” on the isochrones corresponding to the onset of nuclear reactions in the shells of the stars when they become subgiants and swiftly redden. We see a considerable number of stars rightward of the 400-Myr isochrone, i.e., A stars.

The dashed line in Fig. 1b indicates the adopted calibration

$$M_{V_T} = -20.749(B_T - V_T)_0^4 - 22.376(B_T - V_T)_0^3 - 7.2134(B_T - V_T)_0^2 + 6.3192(B_T - V_T)_0 + 1.32. \quad (5)$$

It is semiempirical, reflecting a different fraction of stars deviated from the ZAMS (the 1-Myr isochrone) for different $(B_T - V_T)_0$. Only in the central part of this figure is this fraction large and the calibration deviates noticeably from the ZAMS. The scatter of the 3237 stars under consideration relative to this curve is 0.8^m . This gives r_{ph} with a relative accuracy of 40%. As we see from Fig. 1, this accuracy cannot be higher, because it is determined by the M_{V_T} difference between the 1-Myr isochrone (ZAMS) and the loops of the isochrones (the making of a subgiant).

The distances r_{ph} are important in our study, because the preliminary sample and the sample produced below contain only 9926 (26%) and 5605 (27%) Hipparcos stars, respectively, with the accuracy of their r_{HIP} being higher than 40%. Thus, for the overwhelming majority of the stars under consideration, r_{HIP} are either lacking or less accurate than r_{ph} .

Reconciling M_{V_T} , r_{ph} and A_{V_T}

Below, we perform the main procedure of our study – a mutually reconciled refinement of M_{V_T} , r_{ph} and A_{V_T} by iterations, given the mentioned dependences of these quantities on one another. Since the variations and errors in A_{V_T} are small compared to those for M_{V_T} and r_{ph} , the calculations converge with confidence and reach a relative computational accuracy of 0.001 no later than the twentieth iteration for more than 90% of the stars.

The iterations did not converge for giants, supergiants, shell stars, peculiar and late-type stars, because the calibration (5) is invalid for them. One

of the advantages of this approach is that no stars are excluded from the sample in advance.

Out of the stars that passed the iterations, 20 514 have $(B_T - V_T)_0 < 0$ and $M_{V_T} > -5$ (the second condition rejects the OB giants and supergiants that passed the iterations, but the calibration (5) gives unrealistic values for them). They are considered below in this study as the final sample of OB stars near the MS (presumably with an age of less than 400 Myr). Out of these stars, 7526 (37%) are from Hipparcos and 15 734 (77%) have the spectral classification from TST or HIC. Among the classified stars, the distribution in spectral types is the following: O – 73 (0.5%), B – 8494 (54%), A0 – 6165 (39%) A1-A9 – 944 (6%), F – 32 (0.2%), G – 9, K – 17. Thus, 14 732 stars (94% of the classified stars) are of types O-A0, which allows the selection of OB stars to be recognized as successful (some fraction of A stars is present, but it will be useful below for comparison when dividing the sample into age subsamples).

The distances r_{HIP} , r_{rpm} and r_{ph} agree within 350 pc of the Sun; further out, systematic effects have an impact. At great distances, r_{ph} seem to be most accurate.

SPATIAL DISTRIBUTION

Figure 2 shows the distribution of the sample stars in projection onto the XY , XZ , and YZ planes (the X axis is directed toward the Galactic center, the Y axis is in the direction of rotation, the Z axis is directed toward the North Pole, the Sun is at the center, the distances are in kpc): (a) with r_{HIP} for 7288 Hipparcos stars with $\pi > 0$ mas, (b) with r_{rpm} for all 20 514 stars, (c) with r_{ph} for the same stars. We see that the sample from Tycho-2 encloses an appreciably larger space than does the sample from Hipparcos. The Great Tunnel passing from the second octant to the sixth one (Welsh 1991) is clearly seen on the XY plots as a region of low star density near the Sun bounded by concentrations of stars; the Gould Belt (Perryman 2009, pp. 324–328; Gontcharov 2009) is seen on the XZ plots as a region of enhanced star density inclined to the equator approximately by 17° ; the radial (relative to the Sun) regions of reduced star density produced by extinction in the nearest clouds near the equator and in the Gould Belt are seen on all plots; on plots (b), in contrast to (a) and (c), the radial (relative to the Sun) concentrations of stars produced by the systematic errors in r_{rpm} are clearly seen. Small

regions of high star density are clearly seen here and there – OB associations and their groups, for example, the associations in Orion ($Y \approx -0.2$ kpc, $Z \approx -0.15$ kpc) are seen on the YZ plot.

The accuracy of the Tycho-2 photometry gives hope that the theoretical correlation between the age and $(B_T - V_T)_0$ for OB stars near the MS seen in Fig. 1 will manifest itself if we divide our sample into three $(B_T - V_T)_0$ subsamples: (1) 5141 stars with $(B_T - V_T)_0 < -0.2^m$, (2) 6561 stars with $-0.2^m < (B_T - V_T)_0 < -0.1^m$, and (3) 8812 stars with $-0.1^m < (B_T - V_T)_0 < 0^m$ (below, the subsamples are mentioned under numbers 1–3). The subsamples must contain mostly stars with ages younger than 100, 100–200, and 200–400 Myr, respectively, and, consequently, must have different spatial distributions and kinematics. However, the age of a specific star can be estimated from its $(B_T - V_T)_0$ only with a relative error of 50–100%. Therefore, here only the mean age of the subsample stars and the age– $(B_T - V_T)_0$ correlation make sense.

Figure 3 shows the expected large difference in the distributions of the subsamples in projection onto the XY , XZ , and YZ planes (the designations are the same as those in Fig. 2).

The stars older than 200 Myr form an almost flat layer along the equator with a uniform distribution of stars inside it (the small bend on the XZ plot (c) results from the observational selection due to extinction in the Gould Belt), showing no evidence of the Gould Belt, the Local Bubble, the Great Tunnel, and other present-day structures. These structures are clearly seen on plot (b) and especially on plot (a). In the last 100 Myr, the layer of stars has been strongly deformed, especially along the Z axis. In fact, the stars on plot (a) form a single 3D saddle-shaped structure including the Gould Belt. This structure is asymmetric relative to the Sun: the stars prevail in the southern Galactic hemisphere, in the fourth and especially the third quadrants (for example, the group of associations in Orion).

These peculiarities of the distribution of young stars are seen when analyzing the Z distribution of stars. For all subsamples, this distribution is well fitted by a barometric law $D_0 \cdot e^{-|Z+Z_0|/Z_H}$, where D_0 is the density in the plane of the maximum, Z_0 is the height of the Sun above this plane, Z_H is the distance from this plane at which the density decreases by a factor of e or the half-thickness of a homogeneous layer of stars (Parenago 1954, p. 264). The BMG fit is much poorer. The results found by the least squares method using r_{HIP} or r_{ph} with the limitation $(X^2 + Y^2)^{1/2} < 350$ pc for the sample to be complete and without it are presented in the table. Note that

the number of stars with r_{HIP} is appreciably smaller than that of stars with r_{ph} .

Table 1: Parameters Z_H and Z_0 when the Z distribution of stars is fitted by the barometric law.

Subsample	$(X^2 + Y^2)^{1/2} < 350$		Without limitation	
	r_{HIP}	r_{ph}	r_{HIP}	r_{ph}
Z_H , pc:				
1 $((B_T - V_T)_0 < -0.2)$	50	60	90	160
2 $(-0.2 < (B_T - V_T)_0 < -0.1)$	60	55	75	70
3 $(-0.1 < (B_T - V_T)_0 < 0)$	60	55	75	65
Z_0 , pc:				
1 $((B_T - V_T)_0 < -0.2)$	30	30	45	75
2 $(-0.2 < (B_T - V_T)_0 < -0.1)$	22	17	30	15
3 $(-0.1 < (B_T - V_T)_0 < 0)$	10	15	13	10

The parameter Z_H corresponds to the thickness estimates for the layer of youngest Galactic stars, except for Z_H for subsample 1 without any distance limitation. The large values of Z_0 for subsamples 1 and 2 suggest a large vertical displacement of the layer of stars (and gas producing stars) in the last 200 Myr. The Gould Belt results from this displacement. It explains the value of $Z_0 \approx 25$ pc usually obtained when analyzing young stars (Maiz-Apellaniz 2001). Z_0 for subsample 3 (10 – 15 pc) corresponds to 13 ± 2 found by Gontcharov (2008b, 2011) when analyzing the spatial distribution of red giant clump and branch stars, respectively. Thus, when calculating and mentioning the height of the Sun above the Galactic equator, it is necessary to specify relative to which stars this height is considered. The height seems to change smoothly with stellar age, because the height of the Sun above the layer of the medium producing stars changed with time.

A large number of regions of enhanced star density (like the mentioned group of associations in Orion) can be seen in Figs. 3a and 3b. The produced sample allows these structures to be analyzed in future by taking into account the stellar ages.

KINEMATICS

Out of the 20 514 sample stars, 2293 stars have radial velocities V_r from the Pulkovo Compilation of Radial Velocities (PCR_V, Gontcharov 2006) and the RAVE catalog (Steinmetz et al. 2006). Since only eight stars from them do not enter into Hipparcos, to avoid the influence of a few distant stars, we limited the sample by the condition $r_{ph} < 350$ pc (1954 stars remained) or $r_{HIP} < 350$ pc (1557 stars), depending on whether r_{ph} or r_{HIP} was used. All our kinematic results were obtained with both r_{ph} and r_{HIP} . Although a small fraction of the sample stars have V_r , our subsequent conclusions about the kinematics seem to be valid for the entire sample, because the distributions of the stars with V_r , in space, in $(B_T - V_T)_0$, and in M_{V_T} correspond to the distributions of all sample stars.

The distributions of the stars with V_r over subsamples 1, 2, 3 are: 245, 565, 747 stars with $r_{HIP} < 350$ pc and 266, 748, 940 stars with $r_{ph} < 350$ pc, respectively. However, we used the division into the subsamples only when analyzing the distribution of the stars in the space of velocities UVW . When the velocity dispersions, components of the solar motion to the apex, and Ogorodnikov–Milne model parameters are calculated, modern computers allow one to apply a moving calculation instead of the calculations of kinematic parameters for a few subsamples and to see their smooth changes with $(B_T - V_T)_0$ and, hence, with stellar age. This approach is analogous to a moving averaging. The stars are lined up in $(B_T - V_T)_0$ and the kinematic parameters are calculated for 200 stars with minimum $(B_T - V_T)_0$. The star with minimum $(B_T - V_T)_0$ is then excluded from the set of stars under consideration, a previously unused star with minimum $(B_T - V_T)_0$ is introduced instead of it, and the calculations are repeated. As a result, we obtain 1754 and 1357 solutions, the sets of kinematic parameters (dispersions, components of the motion to the apex, and Ogorodnikov–Milne model parameters), using r_{ph} and r_{HIP} , respectively.

In Fig. 4, the velocity dispersions (a) $\sigma(U)$, (b) $\sigma(V)$, and (c) $\sigma(W)$ are plotted against $(B_T - V_T)_0$. The gray polygonal line with the step at $(B_T - V_T)_0 = -0.15^m$ indicates the dispersions adopted in the BMG under the assumption that an age of 150 Myr corresponds to the step. The black dashed line indicates the dependence for the initial set of stars. The sharp peaks of the dotted line are due to the presence of a few halo and thick-disk stars (hot subdwarfs, blue horizontal-branch stars) and extremely fast OB stars of an unclear nature. A star was assigned to such runaways and was

excluded from further consideration if at least one of the following conditions was met for it:

$$\begin{aligned}\bar{U} - 3\sigma(U_{BMG}) &< U < \bar{U} + 3\sigma(U_{BMG}) \\ \bar{V} - 3\sigma(V_{BMG}) &< V < \bar{V} + 3\sigma(V_{BMG}) \\ \bar{W} - 3\sigma(W_{BMG}) &< W < \bar{W} + 3\sigma(W_{BMG}),\end{aligned}$$

where \bar{U} , \bar{V} , \bar{W} are the mean values of U , V , W for the corresponding $(B_T - V_T)_0$; $\sigma(U_{BMG}) = 67$, $\sigma(V_{BMG}) = 51$, $\sigma(W_{BMG}) = 42$ km s⁻¹ are the velocity dispersions for the thick disk from the BMG. In our analysis based on r_{ph} and r_{HIP} , we excluded 61 (3%) and 29 (2%) runaways, respectively. The dependence of the dispersions on $(B_T - V_T)_0$ after the elimination of runaways is indicated by the gray and black curves for r_{HIP} and r_{ph} , respectively. The lightgray vertical lines indicate the formal accuracy of the dispersion estimated from r_{HIP} (the accuracy from r_{ph} is slightly higher). The black triangles with error bars indicate the result from Torra et al. (2000). The filled square with error bars indicates the result from Dehnen and Binney (1998). Unfortunately, for the remaining dispersion estimates encountered in the literature, either the stellar ages cannot be established or the results refer to a very wide range of ages. The conclusions are the following.

- The results for the two types of distances agree within the formal accuracy almost everywhere and also agree with the results of other researchers.
- Both in the results obtained here and in the results of other authors, we see systematic variations of the dispersions with $(B_T - V_T)_0$ and, apparently, with stellar age.
- The approximation of a stepwise change in dispersions with age adopted in the BMG is too rough and inaccurate, especially for the bluest (youngest) stars. We see that the BMG dispersions more likely correspond to those of the initial set. The presence of an admixture of runaways among the young stars seems to have been disregarded in the BMG.
- The elimination of a few runaways changed radically the result. Therefore, it is necessary to thoroughly study the nature of these stars, to determine the characteristics of their population, and to justify the criteria for their elimination.

- For the youngest stars ($(B_T - V_T)_0 < -0.23^m$), the dispersions increase, confirming the previously detected (Fig. 3 and the table) large deformation of the layer of stars along the Z axis in the last 100 Myr with the formation of the Gould Belt.
- The dispersion $\sigma(W)$ changes approximately periodically. It should be checked whether this is a real effect or an artifact.

After the elimination of runaways, let us consider the distribution of the stars from subsamples 1–3 in velocity space in projection onto the UV , UW , and VW planes (km s^{-1}). Figures 5a, 5b, and 5c for subsamples 1, 2, and 3, respectively, show UVW obtained with r_{HIP} and r_{ph} , which give similar results. Not only an increase in the velocity dispersions with age, but also significant differences in the distributions of the subsamples are clearly seen. They agree with the analogous results from Antoja et al. (2008) presented in their Fig. 13: plot (a) with their plot for stars younger than 100 Myr, plot (c) with their plot for 100 – 500 Myr, and plot (b) is intermediate in appearance. As expected, the change in the number of stars belonging to the four main superclusters/ streams (marked in Fig. 5 by the corresponding numbers) is most pronounced in the UVW space within the last 400 Myr:

1. The Pleiades ($U \approx -12$, $V \approx -22 \text{ km s}^{-1}$; U , V , W for the groups here and below were taken from Antoja et al. (2008) and Bobylev et al. (2010)) is clearly seen on all plots in accordance with the cluster age of about 100 Myr (Bovy and Hogg 2010).
2. Coma Berenices ($U \approx -10$, $V \approx -5 \text{ km s}^{-1}$), as expected, is appreciably outnumbered by the Pleiades in the number of stars on plot (a) and is clearly seen on (b) and (c).
3. UrsaMajor or the Sirius stream ($U \approx +9$, $V \approx +3 \text{ km s}^{-1}$) is absent on plot (a), manifests itself as isolated stars on (b), and dominates on (c) in accordance with the cluster age estimate, 350 – 413 Myr (Bovy and Hogg 2010).
4. The Hyades ($U \approx -40$, $V \approx -20 \text{ km s}^{-1}$) manifests itself only as isolated stars on plot (c) in accordance with the cluster age, 488 – 679 Myr (Bovy and Hogg 2010).

Naturally, the derived distribution differs noticeably from that for older stars, giants (Famaey et al. 2005), and main-sequence F and G stars (Nordström et al. 2004); for example, the Hercules stream ($U \approx -30$, $V \approx -50$ km s⁻¹) is absent here.

Let us determine the kinematics of OB stars within the framework of the linear Ogorodnikov–Milne model described by Gontcharov (2011). As has been noted above, the model parameters (the solar motion components relative to the stars U_{\odot} , V_{\odot} , W_{\odot} , the partial derivatives of the velocity with respect to the distance $M_{ux} - M_{wz}$, the Oort constants A , B , C , K , the vertex deviation l_{xy} , and the angular velocity of Galactic rotation Ω_{R0}) were determined by moving calculations, which allows their change with $(B_T - V_T)_0$ to be traced.

In Fig. 6, the solar motion components (a) U_{\odot} , (b) V_{\odot} , (c) W_{\odot} relative to the stars are plotted against $(B_T - V_T)_0$: just as in Fig. 4, the gray curve for r_{HIP} and the black curve for r_{ph} ; the accuracy of the result from r_{HIP} is indicated by the light-gray vertical lines. For comparison, the black triangles, gray square, gray circle, black diamond, black circles, and black square (not the popular (in references) mean solar motion relative to MS stars of different ages but the result for blue stars) indicate, respectively, the results from Torra et al. (2000), Bobylev (2006), Zabolotskikh et al. (2002), Glushkova et al. (1998), Elias et al. (2006), and Dehnen and Binney (1998). Here, as in our analysis of the dispersions in Fig. 4, there is agreement of the results from the two types of distances between themselves and with those of other researchers and smooth systematic variations with $(B_T - V_T)_0$ are seen in all results.

While analyzing the discrepancies, we should note $W_{\odot} = 12$ km s⁻¹ from Glushkova et al. (1998). This value is not shown in the figure, because it differs significantly from the remaining values apparently due to the use of only μ and/or due to the difference between the spatial regions of the samples. There is also a clear discrepancy between the results obtained and $U_{\odot} = 12$ km s⁻¹ from Dehnen and Binney (1998) (the black square on plot (a)). The use of only μ is apparently also responsible for this discrepancy, which can give a systematic error in the presence of radial streams of young stars in the Galaxy. The results from Elias et al. (2006) marked on each plot by four black circles, two for μ and two for V_r , are an example of the difference in the results when using only μ and only V_r : U_{\odot} agree, while V_{\odot} and W_{\odot} disagree noticeably. It can be suggested that V_{\odot} and W_{\odot} are closer to the true value when using V_r (larger values in this case) and μ (smaller

values), respectively, in accordance with the dominant contribution of the Galactic rotation to each velocity component. The results from Elias et al. (2006) then agree well with our results.

For the stars with $(B_T - V_T)_0 < -0.22^m$, i.e., the Gould Belt stars, the behavior of U_\odot and V_\odot changes due to the overall motion of the Gould Belt in the direction of the third Galactic quadrant.

In Fig. 7, the Ogorodnikov–Milne model parameters derived here are plotted against $(B_T - V_T)_0$. For comparison, the triangles indicate the results from Torra et al. (2000): we see their agreement with our results. Unfortunately, in the remaining range of $(B_T - V_T)_0$, there are no other results for comparison. Therefore, the large variations in parameters seen in Fig. 7, especially in the range $-0.13^m < (B_T - V_T)_0 < 0^m$, need to be confirmed by other studies.

The parameters M_{wx} and M_{wy} provide an estimate of the accuracy of our results. They must be small, because the OB stars retain a small thickness of their layer over hundreds of Myr and, hence, have no significant systematic vertical motions, with the possible exception of sample compression/expansion (M_{wz}). We see from the figure that the M_{wx} and M_{wy} variations lie within the error band and do not differ significantly from zero. The variations in M_{vy} , which reflects the sample compression/expansion along the Y axis, are also insignificant.

The variations in the remaining parameters are significant and occasionally correlated between themselves. For example, at $(B_T - V_T)_0 \approx -0.13^m$, i.e., about 170 Myr ago, several parameters change abruptly and since then they have changed monotonically: the M_{ux} variations show that the sample expands after its maximum compression along X ; M_{wz} – periodic expansions and compressions along Z arise after 200 Myr of rest, M_{vz} – a period of constant negative values comes after abrupt changes, a result of the emergence of streams displaced along Z relative to the Sun and having systematic motions along Y (for example, the Pleiades), M_{uy} ($= -\Omega_{R0}$) – the Galactic rotation velocity increases, C and L_{xy} – the rotation of the velocity ellipsoid, the redistribution of the energy of horizontal stellar motions along X into the energy of vertical motions along Z , K – the long period of negative values is replaced by a long period of approximately zero values.

We see that the well-known negative K-effect for OB stars (Bobylev 2006) refers only to the stars in the range $-0.13^m < (B_T - V_T)_0 < -0.05^m$, i.e., with ages of about 170 – 300 Myr.

CONCLUSIONS

This study is the next step in using multicolor broadband photometry following the selection and analysis of the spatial distribution of stars of different types (Gontcharov 2008a, 2008b, 2011) and the construction of 3D maps of reddening, extinction coefficient R_V (Gontcharov 2012a), extinction (Gontcharov 2012b), and a 3D extinction model (Gontcharov 2009) – here, we made an attempt to reconcile the photometric distances, absolute magnitudes, and extinctions for a large number of stars of the same type. The evidence for a successful solution of this problem includes: good agreement of the trigonometric, photoastrometric, and photometric distances within 350 pc of the Sun; the falling of the stars under consideration into the region of the H–R diagram predicted by the theory, between the zero-age main sequence and the beginning of the subgiant stage, after their dereddening; agreement with the well-known spectral classification, according to which O–A0 stars account for 94% of the sample; the division of the sample into three theoretically justified subsamples by the dereddened color $(B_T - V_T)_0$ correlating with the stellar age (less than 100, 100 – 200, and 200 – 400 Myr) and the detection of expected significant differences in the spatial distributions and kinematics of the subsamples; the manifestation of well-known Galactic structures in the spatial distribution – the Great Tunnel, the Gould Belt, the group of associations in Orion, and others; the manifestation of well-known streams (the Pleiades, Coma Berenices, Ursa Major, the Hyades) in the corresponding age subsamples; the manifestation of a unified process in the spatial distribution and kinematics – the replacement of the compression of the sample along the X axis by its deformation along the Z axis 100 – 200 Myr ago with the formation of spatial structures, including the Gould Belt, outside the equatorial plane of the Galaxy; the systematic temporal variations in kinematic parameters of stars (the velocity dispersions, the solar motion to the apex, the Oort constants A , B , C , K , and the Ogorodnikov–Milne model parameters) consistent with the results of other authors. The detection of temporal variations in kinematic parameters is the main result of our study, showing that it is meaningless to calculate these parameters for a sample of stars with uncertain ages or with a wide range of ages.

ACKNOWLEDGMENTS

In this study, we used results from the Hipparcos and 2MASS projects and resources of the Strasbourg Data Center (France), <http://cds.u-strasbg.fr/>. The study was supported by Program P.21 of the Presidium of the Russian Academy of Sciences.

References

1. T. Antoja, F. Figueras, D. Fernandez, et al., *Astron. Astrophys.* **490**, 135, (2008).
2. G. Bertelli, L. Girardi, P. Marigo, et al.), *Astron. Astrophys.*, **484**, 815, (2008).
3. V.V. Bobylev, *Astron. Lett.* **32**, 816 (2006).
4. V.V. Bobylev, A. T. Bajkova, A. A. Muylari, *Astron. Lett.* **36**, 27 (2010).
5. J. Bovy, D.W. Hogg, *Astrophys. J.* **717**, 617, (2010).
6. W. Dehnen, J. Binney, *Mon. Not. R. Astron. Soc.* **294**, 429, (1998).
7. F. Elias, E.J. Alfaro, J. Cabrera-Cano, *Astron. J.* **132**, 1052, (2006).
8. ESA, *Hipparcos and Tycho catalogues* (ESA, 1997).
9. B. Famaey, A. Jorissen, X. Luri, et al., *Astron. Astrophys.* **430**, 165, (2005).
10. E.V. Glushkova, A.K. Dambis, A.M. Mel'nik, et al., *Astron. Astrophys.* **329**, 514, (1998).
11. G. A. Gontcharov, *Astron. Lett.* **32**, 795 (2006).
12. G. A. Gontcharov, *Astron. Lett.* **34**, 7 (2008a).
13. G. A. Gontcharov, *Astron. Lett.* **34**, 785 (2008b).
14. G. A. Gontcharov, *Astron. Lett.* **35**, 780 (2009).
15. G. A. Gontcharov, *Astron. Lett.* **37**, 707 (2011).

16. G. A. Gontcharov, *Astron. Lett.* **38**, 15 (2012a).
17. G. A. Gontcharov, *Astron. Lett.* **38**, 87 (2012b).
18. G.A. Gontcharov, A.T. Bajkova, P.N. Fedorov, et al., *Mon. Not. R. Astron. Soc.* **413**, 1581, (2011).
19. E. Høg, C. Fabricius, V.V. Makarov, et al., *Astron. Astrophys.* **355**, L27, (2000).
20. F. van Leeuwen, *Astron. Astrophys.* **474**, 653, (2007).
21. T.E. Lutz, D.H. Kelker, *Publ. Astron. Soc. Pacif.* **85**, 573, (1973).
22. J. Maiz-Apellaniz, *Astron. J.* **121**, 2737, (2001).
23. P. Marigo, L. Girardi, A. Bressan, et al., *Astron. Astrophys.* **482**, 883 (2008).
24. B. Nordström, M. Mayor, J. Andersen, et al., *Astron. Astrophys.* **418**, 989 (2004).
25. P. P. Parenago, *A Course of Stellar Astronomy* (GITTL, Moscow, 1954) [in Russian].
26. M. Perryman, *Astronomical Applications of Astrometry* (Cambridge Univ. Press, Cambridge, 2009).
27. G.H. Rieke, R.M. Lebofsky, *Astrophys. J.* **288**, 618, (1985).
28. A.C. Robin, C. Reyle, S. Derriere, et al., *Astron. Astrophys.* **409**, 523, (2003).
29. M.F. Skrutskie, R.M. Cutri, R. Stiening, et al., *Astron. J.* **131**, 1163, (2006).
30. M. Steinmetz, T. Zwitter, A. Siebert, et al., *Astron. J.* **132**, 1645, (2006).
31. N. Tetzlaff, R. Neuhauser, M.M.Hohle, *Mon. Not. R. Astron. Soc.* **410**, 190, (2011).
32. J. Torra, D. Fernandez, F. Figueras), *Astron. Astrophys.* **359**, 82, (2000).

33. C. Turon, M. Cr ez e, D. Egret, et al., Bull. Inform. CDS **43**, 5, (1993).
34. B.Y. Welsh, Astrophys. J. **373**, 556, (1991).
35. C.O. Wright, M.P. Egan, K.E. Kraemer, et al., Astron. J. **125**, 359, (2003).
36. M. V. Zabolotskikh, A. S. Rastorguev, and A. K. Dambis, Astron. Lett. **28**, 454 (2002).

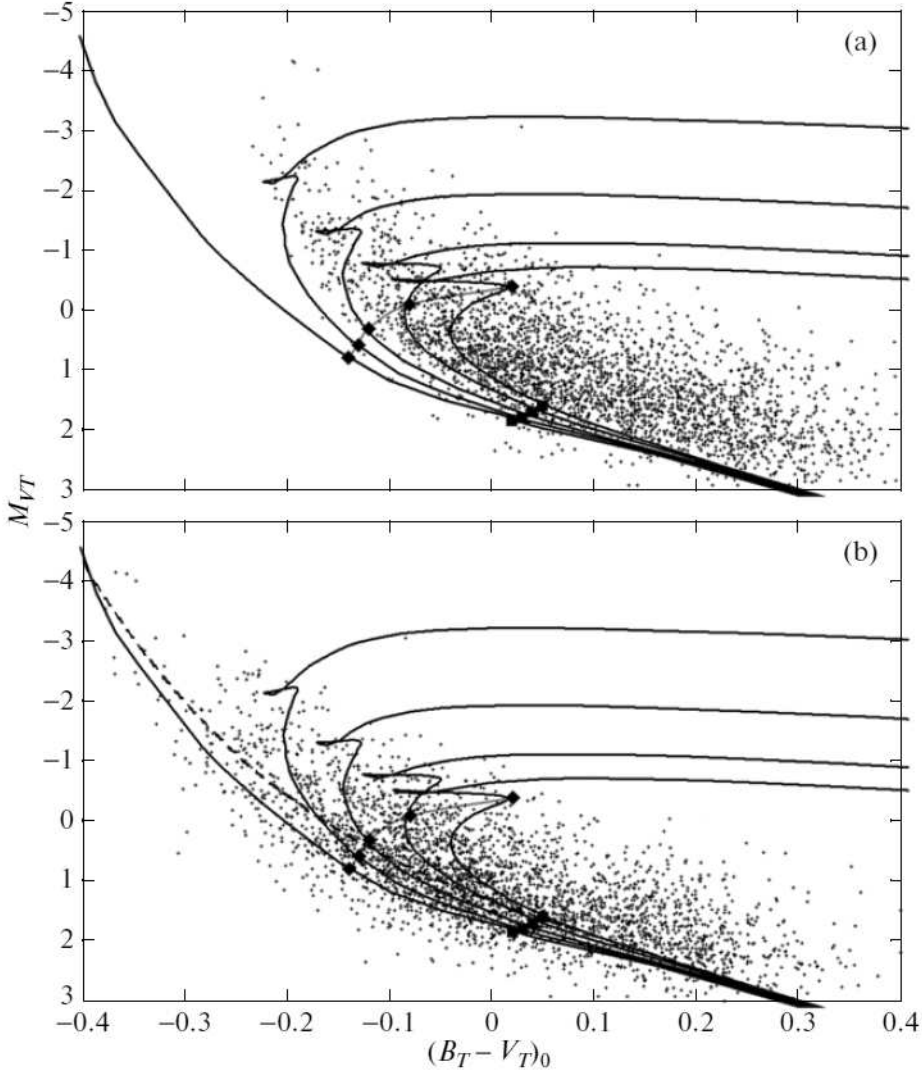


Figure 1: H–R diagram. The theoretical isochrones for solar-metallicity stars with ages of 1, 100, 200, 300, and 400 Myr are indicated by five black curves from left to right. The theoretical evolutionary tracks for solar-metallicity stars with masses of $2.9 M_\odot$ and $2 M_\odot$ are indicated by the diamonds with the gray curve and the squares, respectively. The 3237 Hipparcos stars from the preliminary sample with $\pi > 5$ mas and $\sigma(\pi)/\pi < 0.2$ are indicated by the crosses before (a) and after (b) their dereddening. The adopted calibration is indicated by the black dashed line.

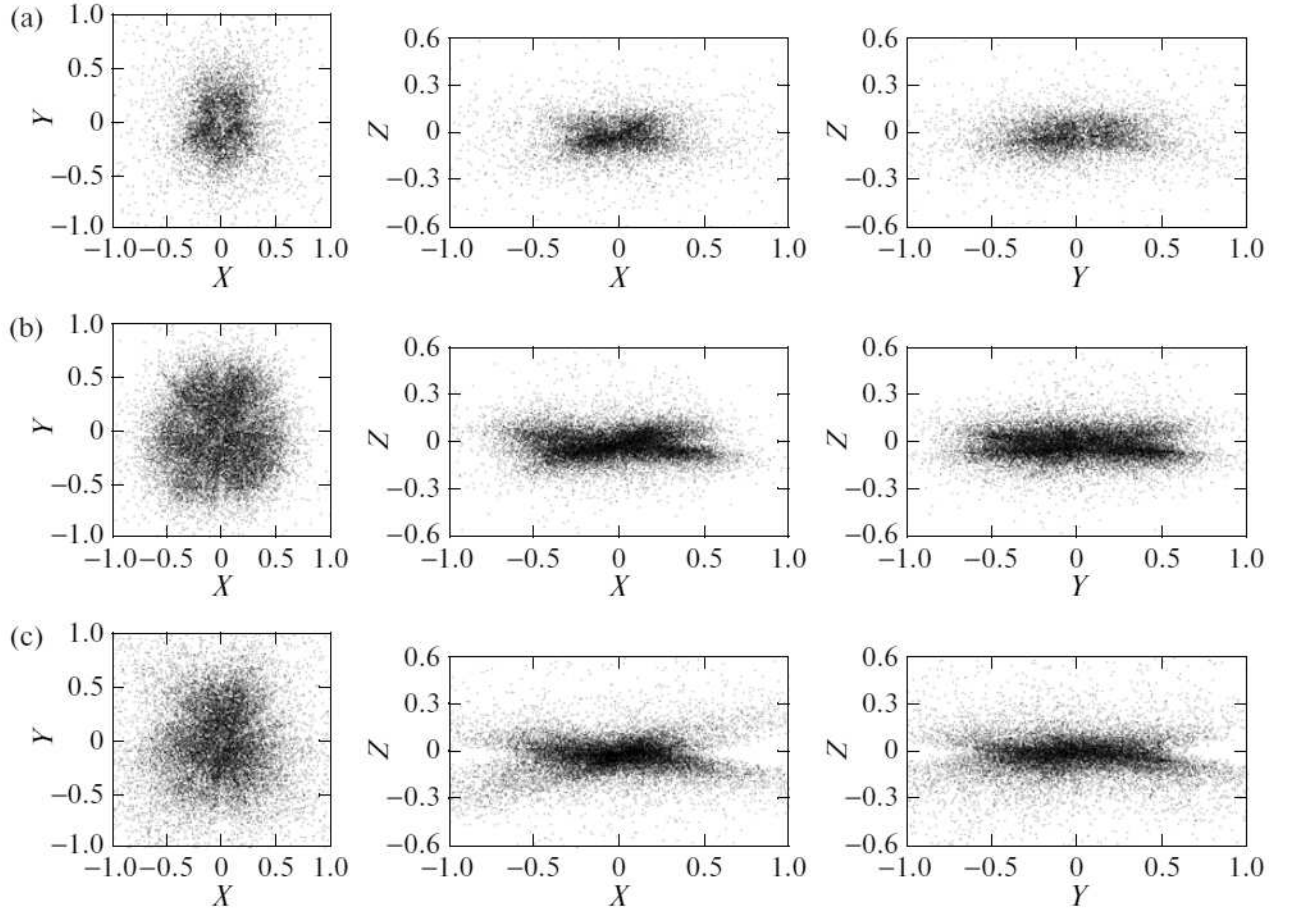


Figure 2: Distribution of the sample stars in projection onto the XY , XZ , and YZ planes (distances in kpc): (a) with r_{HIP} for Hipparcos stars, (b) with r_{rpm} for all 20 514 stars, and (c) with r_{ph} for them.

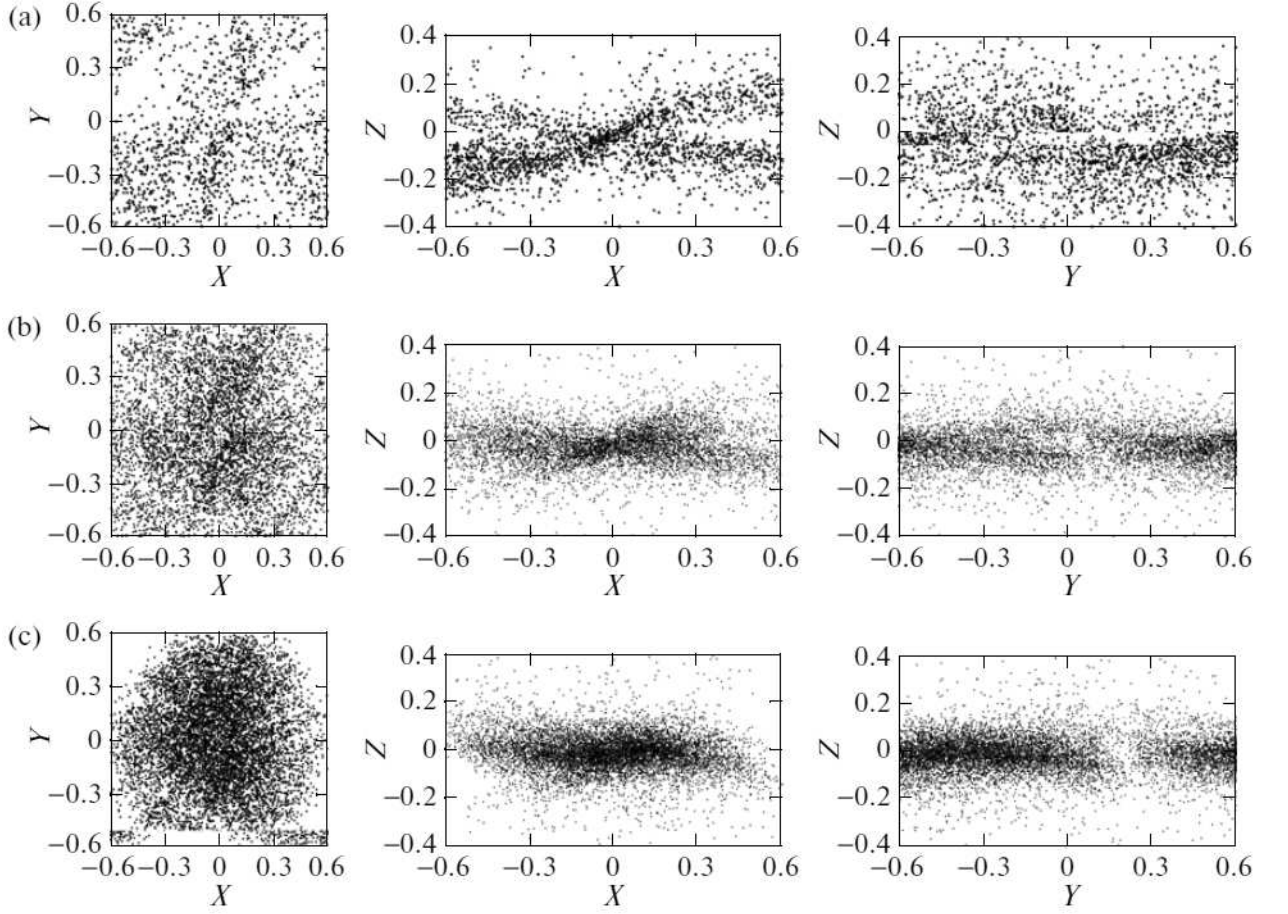


Figure 3: Distribution of the stars from subsamples 1–3 in projection onto the XY , XZ , and YZ planes (distances in kpc): (a) $(B_T - V_T)_0 < -0.2^m$ (younger than 100 Myr), (b) $-0.2^m < (B_T - V_T)_0 < -0.1^m$ (100 – 200 Myr), and (c) $-0.1^m < (B_T - V_T)_0 < 0^m$ (200 – 400 Myr).

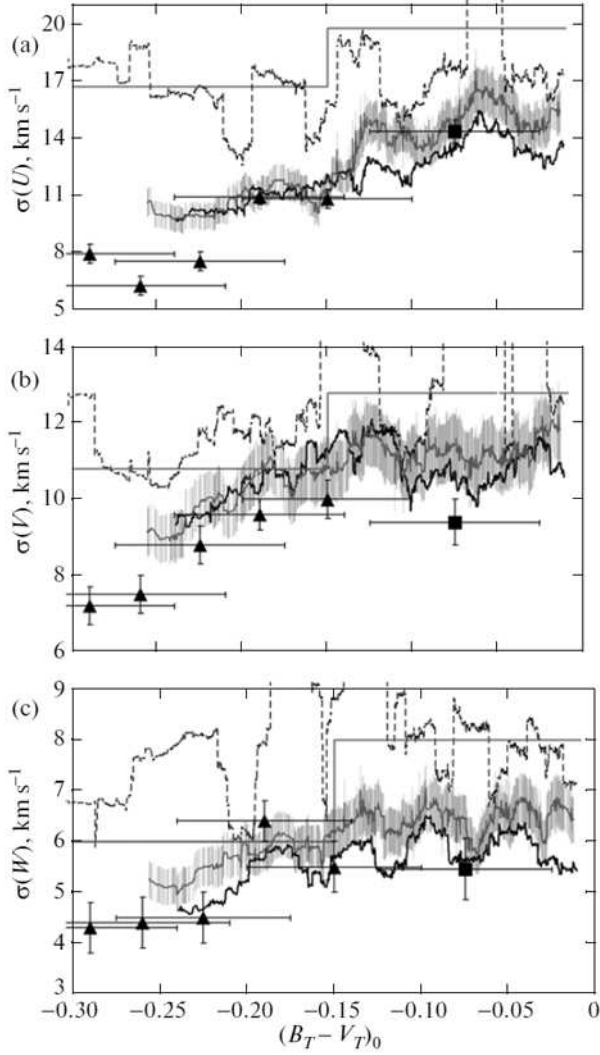


Figure 4: Dependences of (a) $\sigma(U)$, (b) $\sigma(V)$, and (c) $\sigma(W)$ (km s^{-1}) on $(B_T - V_T)_0$. The dispersions from the BMG are indicated by the gray curve with one step corresponding to an age of 150 Myr. The dependence for the initial set of stars is indicated by the black dashed line. The dependence after the elimination of runaway stars is indicated by the gray curve for r_{HIP} and by the black curve for r_{ph} . The accuracy of the result for r_{HIP} is indicated by the light-gray vertical lines. The result from Torra et al. (2000) is represented by the black triangles. The result from Dehnen and Binney (1998) is represented by the black square.

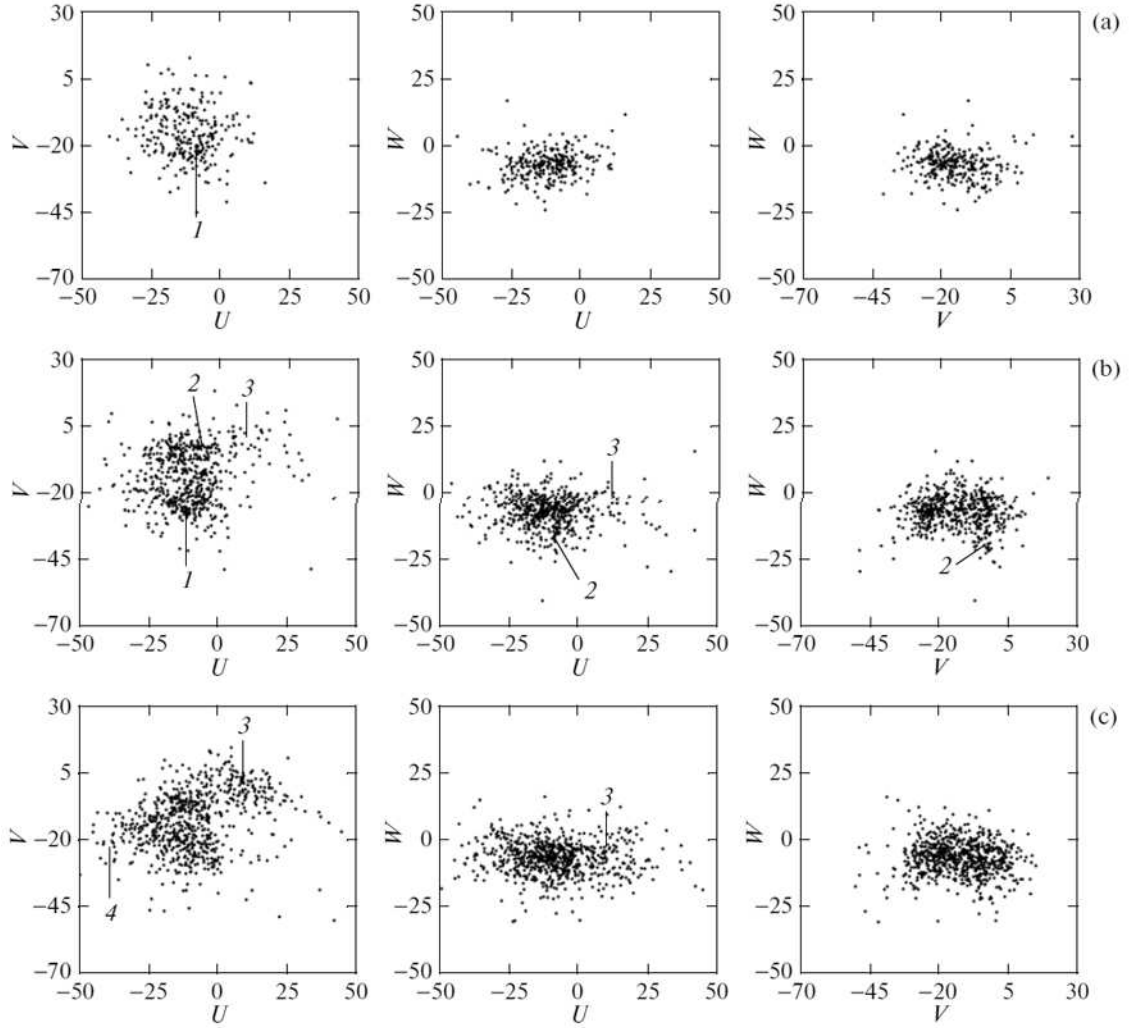


Figure 5: Distribution of the subsample stars on the UV , UW , and VW diagrams: (a) 1, (b) 2, (c) 3 (velocities in km s^{-1}). The numbers mark the groups discussed in the text.

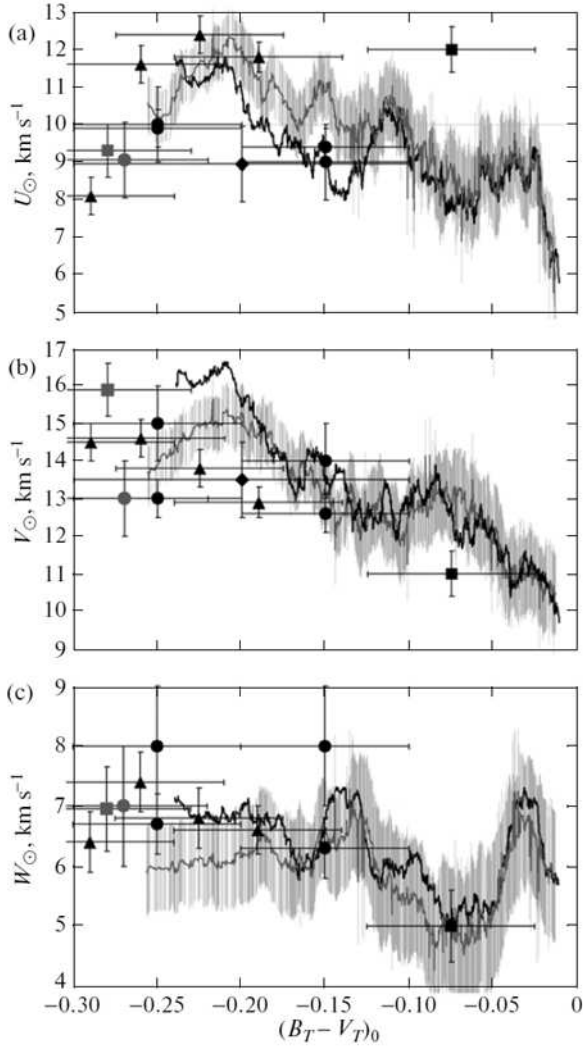


Figure 6: (a) U_{\odot} , (b) V_{\odot} , and (c) W_{\odot} (km s^{-1}) versus $(B_T - V_T)_0$: the gray curve for r_{HIP} and the black curve for r_{ph} . The accuracy of the result from r_{HIP} is indicated by the light-gray vertical lines. The results from Torra et al. (2000), Dehnen and Binney (1998), Bobylev (2006), Zabolotskikh et al. (2002), Glushkova et al. (1998) (no W_{\odot}), and Elias et al. (2006) are indicated by the black triangles, black square, gray square, gray circle, black diamond, and black circles, respectively.

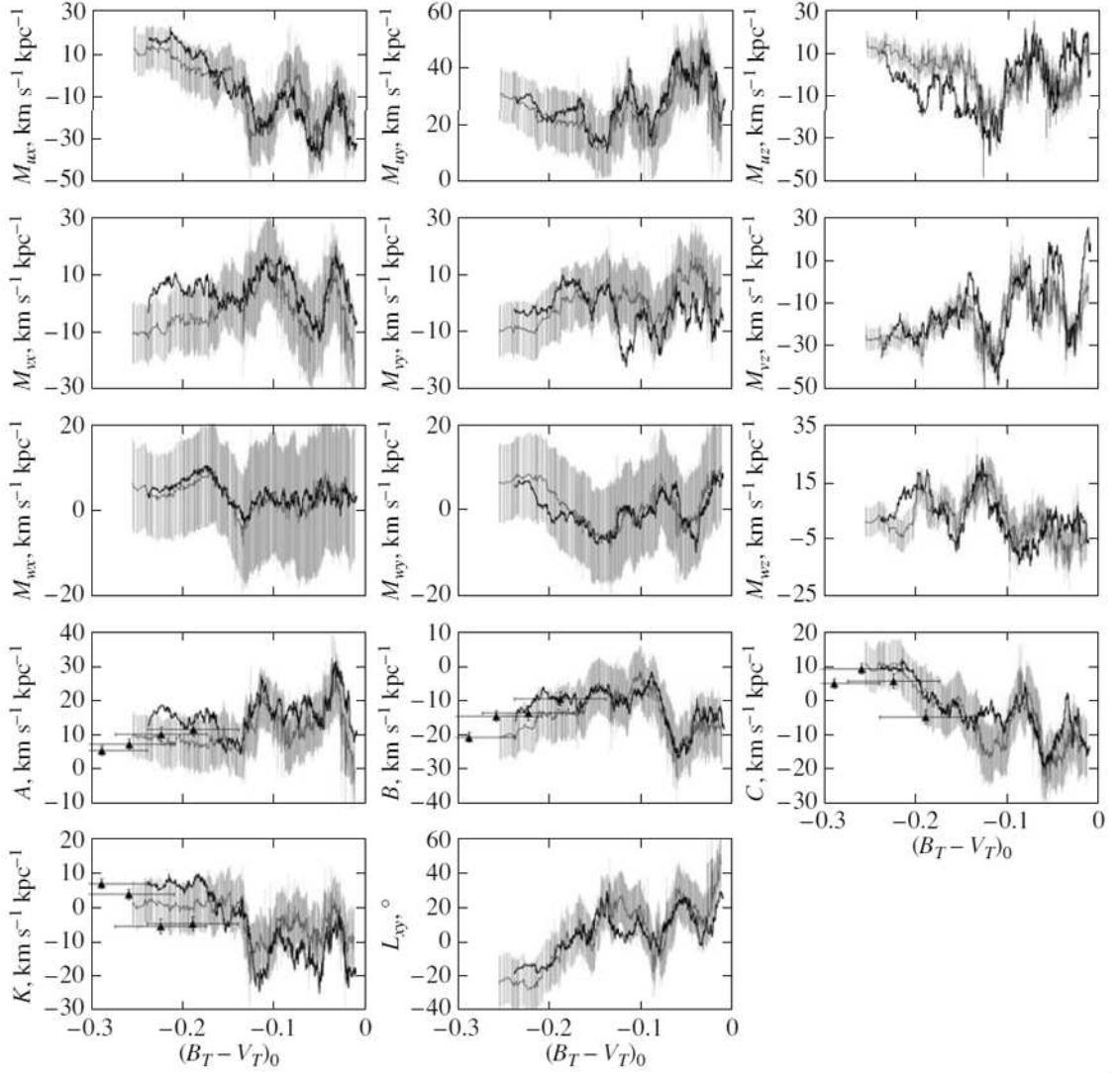


Figure 7: Ogorodnikov–Milne model parameters versus $(B_T - V_T)_0$: the gray curve for r_{HIP} and the black curve for r_{ph} . The accuracy of the result from r_{HIP} is indicated by the light-gray vertical lines. The results from Torra et al. (2000) are indicated by the black triangles.